



First-principles molecular dynamics simulation of O₂ reduction on nitrogen-doped carbon

Yasuhiro Okamoto ^{a,b}

^a Nanoelectronics Research Laboratories, NEC Corporation, 34 Miyukigaoka, Tsukuba, Ibaraki 305-8501, Japan

^b Institute for Solid State Physics, University of Tokyo, 5-5-5 Kashiwanoha, Kashiwa, Chiba 277-8581, Japan

ARTICLE INFO

Article history:

Received 28 January 2009

Received in revised form 5 August 2009

Accepted 10 August 2009

Available online 14 August 2009

ABSTRACT

Density-functional calculations were performed to examine oxygen reduction reactions (ORRs) on N-doped graphene sheets. We found that O₂ adsorption becomes energetically favorable as the number of N around a C=C bond increases. Pathways for both 4e⁻ and 2e⁻ reductions were identified. The possibility of O poisoning was suggested after calculating the reversible potential of each reduction step.

© 2009 Elsevier B.V. All rights reserved.

Keywords:

First-principles
Density-functional theory
Ab initio
Oxygen reduction
Fuel cell
Cathode
Carbon
Nitrogen

1. Introduction

The oxygen reduction reaction (ORR) is a fundamental reaction in electrochemistry [1], and it is commonly observed in nature as the partner reaction in wet corrosion. ORR also occurs in the cathodes of polymer electrolyte membrane fuel cells (PEMFCs) [2,3]. In ORR under an acidic environment, when one O₂ molecule is completely reduced to two H₂O molecules, the reaction is normal and called “4e⁻ reduction” because four electrons are involved in the process. On the other hand, when the O₂ reduction is incomplete and terminates in the formation of HOOH, the reaction is unfavorable and called “2e⁻ reduction”.

Because cathodic reactions of PEMFC occur under high electrode potential (~1 V) and high hydrogen ion concentration (~1 pH), we have to use platinum or platinum alloy as a catalyst for chemical stability and catalytic activity. Moreover, since the total reaction energy of the entire ORR (O₂_{gas} + 4H_{aq}⁺ + 4e⁻ → 2H₂O_{liq}) is fixed, the allocation of the reaction energy to each reduction step brings about trade-offs; if one elementary reaction becomes highly exothermic, the successive one tends to be endothermic. This causes a problem in designing catalysts for ORR.

A catalyst that is free of expensive precious metals such as platinum would be the Holy Grail of ORR. One of the serious

problems of PEMFC is that large amounts of platinum are needed in the cathode because the cathodic reaction is much slower than the anodic one. Platinum-free catalysts for ORR thus have a great impact on the success of PEMFC and have been steadily investigated. ORR on metal phthalocyanines [4] and other organometallic compounds [1] has been studied for many years. However, the catalytic activity of these compounds is significantly lower than that of platinum. Moreover, they have a durability problem because they are not very stable under acidic conditions. Despite these problems, Bashyam and Zelenay [5] fabricated a promising durable catalyst where Co atoms/ions bond with polypyrrole. Polymerization of pyrrole molecules seems to increase the catalyst's stability.

Sidik et al.'s work is also a noteworthy attempt to fabricate a precious metal-free ORR catalyst. They experimentally and theoretically examined O₂ reduction catalysis on nitrogen-doped carbon [6]. Although the reaction mainly proceeds through 2e⁻ reduction on their catalyst, their work may serve as a stimulus to the development of precious metal-free catalysts. Moreover, elucidating the reduction mechanisms of metal-free catalysts such as nitrogen-doped carbons [6] and nitrogen- and boron-doped carbons [7] may be helpful for understanding the necessity of platinum in ORRs.

If we are to find efficient catalysts for PEMFCs, we need to know more about the elementary process of redox reactions on catalysts. Calculations based on density-functional theory (DFT) may provide

E-mail address: y-okamoto@df.jp.nec.com.

such information and might shed new light on the mechanisms of redox reactions. There have been a number of first-principles studies aimed at providing a better understanding of chemical reactions occurring in electrode/water interfaces. These studies include metal/vacuum calculations ignoring the solvent effect, as in a thermodynamic study of water electrolysis on metal surfaces [8], cluster model calculations, e.g., of hydrogen oxidation reactions using a charged metal cluster with “rained down” water molecules [9], static DFT calculations, e.g., of the bias effect on methanol dehydrogenation [10], first-principles molecular dynamics (FPMD) simulations, e.g., of ORR on Pt(111) by a solvated ion ($\text{H}_3\text{O}^+(\text{H}_2\text{O})_2$) [11], and FPMD simulations combined with an effective screening medium (ESM) [12] to control the potential in the double layer region, as was done in studies of the structure of the Pt(111)/ H_2O interface [13], and the Volmer step of H_2 evolution on a Pt(111) surface [14]. Identification of metal dimers that are suitable for catalyzing the ORR on the basis of DFT calculations, and confirmation of the catalysis through FPMD simulations have also been investigated [15].

In this paper, we examined ORR on nitrogen-doped graphene sheets as inspired by the model proposed by Sidik et al. [6]. Although Ikeda et al. showed a possibility of enhanced ORR activity on the zigzag edge of nitrogen-doped graphite by using FPMD simulations [16], nitrogen-doping in a basal plane of graphite may be more favorable than that in edge sites because the number of available doping sites is larger in the basal plane than that in the edge. The main differences between Sidik's model and present one are as follows: The number of nitrogen atoms in our model is different from theirs. This significantly affects the reactivity of graphene sheets. They considered an atomic structure containing one nitrogen atom; we consider structures containing 0–4 nitrogen atoms. The state of O_2 adsorption is different. Judging from the separation of 3.0 Å between an O_2 molecule and the graphene sheet, the O_2 molecule is physisorbed in their model and an oxygen atom of the O_2 is just above a nitrogen atom in the graphene sheet. This might be unfavorable for the O_2 approaching the graphene sheet, because of a repulsive interaction between lone pair electrons of oxygen and nitrogen atoms. By contrast, an O_2 molecule is chemisorbed in our model by avoiding the position just above the nitrogen atom, although the chemisorbed state may be metastable. Another difference is that, in addition to high spin density at C atoms that bond with the N atom, we consider that polarization of C–N bonds plays an important role in ORR on a nitrogen-doped graphene sheet. Doping of electronegative nitrogen atoms reduces the electron density of carbon atoms that bond with nitrogen atoms and polarizes the carbon atoms into δ^+ . Polarization of the C–N bonds makes it easy for dative bonds to form between the carbon atoms and the O_2 molecule.

Our research consists of four phases. First, the formation energy and O_2 adsorption energy of nitrogen-doped graphene sheets were examined by using static DFT calculations. Second, qualitative ORR pathways on the representative N-doped graphene sheets were identified by using FPMD simulations. Third, alternative ORR intermediates that were not found in the FPMD simulation as well as possible branching paths were examined. Finally, the reversible potential of each reduction step was calculated in relation to the determined pathways.

2. Computational method

All first-principles calculations in this paper were performed using the Simulation Tool for the Atom TEchnology (STATE) program package [17]. Calculations of the atomic geometry and electronic structure were made in accordance with the DFT framework within a generalized gradient approximation (GGA) to the exchange-correlation functional formulated by Perdew, Burke,

and Ernzerhof(PBE96) [18]. The ultrasoft pseudopotentials for C, N, O, and H atoms were generated using the process described by Vanderbilt [19]. The partial core correction scheme described by Louie et al. [20] was used for C, N, and O atoms. Plane-wave basis sets with cut-off energies of 25 and 225 Ry were respectively used for the expansion of wave functions and charge density.

The formation energy of N-doped graphene sheets, the adsorption energy of O_2 molecule on the sheets, and the reversible potentials of ORR were examined by using a periodic slab model corresponding to 32 carbon sites (Fig. 1). The calculated C–C bond length of a graphene sheet is 1.425 Å, which is close to the measured value of 1.418 Å.

The FPMD simulations were also performed on a graphene sheet corresponding to 32 carbon sites (Fig. 1) with a water slab composed of 32 H_2O molecules for describing solvent effects. The size of computational cell was $(8.55 \times 9.87 \times 15.88 \text{ \AA}^3)$, and the density of the water slab was $\approx 1 \text{ g/cm}^3$ (considering the volume of the graphite sheet and adsorbate). The cell was the same as the one in previous simulation with respect to the size and the number of solvent molecules in it [15]. A structure of solvent molecules obtained from the previous simulation was used as an initial structure of solution in this simulation, which provides a model of well-equilibrated graphite-water interface. The mass of hydrogen atoms was replaced by that of the deuterium to increase the time step ($\Delta t = 1.21 \text{ fs}$) in the FPMD simulations. Velocity scaling was used to keep the temperature in the FPMD simulations at 353 K. Brillouin zone integration was performed for the $(2 \times 2 \times 1)$ k -points. In our FPMD simulation, the electric potential was applied by putting an H_3O^+ ion keeping the charge neutrality of whole computational cell [15], instead of controlling the excess surface electrons [13,14].

Spin-polarized GGA calculations were made for the formation energy of N-doped graphene sheets, the adsorption energy of an O_2 molecule on the sheets, and the reversible potentials of the ORR on the sheets. FPMD simulations were performed with spin-non-polarized GGA. We expected that ignoring the spin polarization in this case does not substantially change the prediction of the ORR pathways. Although the energy difference between the singlet and triplet of an O_2 molecule isolated in the gas phase is large (~1 eV), the effect of spin polarization on an adsorbed O_2 and the ORR intermediates on the sheets is relatively small. In particular, the results of the spin-polarized calculation of the O_2 adsorption on graphene sheets that contains two or four nitrogen atoms in the computational cell coincided with the results of the spin-non-polarized calculation. This indicates that the effect of spin polarization is small once the O_2 is adsorbed on the graphene sheet.

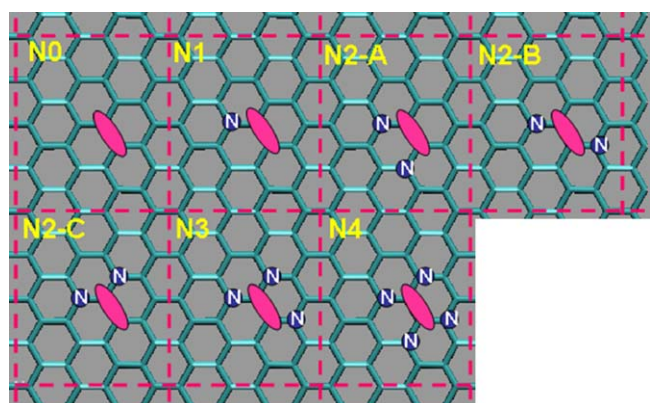


Fig. 1. Model of non-doped graphene sheet (N0) and six N-doped graphene sheets (N1, N2-A, N2-B, N2-C, N3, and N4). Adsorbed O_2 molecules are indicated by red ellipses. (For interpretation of the references to color in this figure legend, the reader is referred to the web version of the article.).

3. Results and discussion

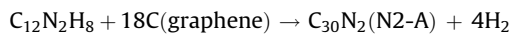
3.1. Formation energy of N-doped carbon

First, the formation energy of six N-doped graphene sheets (Fig. 1) relative to nitrogen molecules plus graphene (E_F) was examined. E_F is defined as follows:

$$E_F = E(C_{32-m}N_m) - (32 - m)\mu_C - \frac{1}{2}m \times \mu_{N_2}$$

Here, $E(X)$ and μ_Y stand for the total energy of X and chemical potential of Y, respectively. We used the total energy of a graphene sheet per atom as μ_C , because GGA functional cannot properly describe attractive interaction between graphite sheets. The formation energies are listed in Table 1. We found that the N2-B model is the most favorable structure in terms of thermodynamics since it has the smallest E_F . Even when we take account of the correction from the Gibbs free energy for N_2 gas in the standard state (0.36 eV/molecule), this model is still the most favorable. The N2-C, N3 and N4 models are less stable than N1 model when the Gibbs free energy correction from N_2 gas is taken into account.

It should be noted that the endothermic formation energy is not unusual. For example, thermochemical data shows that standard formation enthalpy change of pyrazine ($C_4N_2H_4$) is 1.44 and 2.03 eV in crystal and in gas phase, respectively [21]. Moreover, it may be possible to fabricate the less-stable models since using N_2 gas is not the only way to dope graphene with N. Aromatic compounds such as 1,10-phenanthroline and phenazine ($C_{12}N_2H_8$) that contain two N atoms in a six member ring might be helpful for fabricating the N2-A structure shown in Fig. 1. From these molecules, the formation of N2-A model is written as:



Although the reaction energies calculated from the difference of Kohn-Sham (KS) energy between the reactant and product are endothermic by 1.18 (1,10-phenanthroline) and 1.10 eV (phenazine), a consideration of the translational entropy of ideal gas of H_2 (28 cal/(mol K)) makes the products stable at high temperature. Moreover, the KS energy change of the following reaction is exothermic by 1.92 eV.



Note that desorption of an N_2 molecule from the N2-A model is energetically unfavorable, because it leaves six dangling bonds in product. The reaction is highly endothermic (11.95 eV).

3.2. O_2 adsorption energy on N-doped carbon

Next, we examined the O_2 adsorption on N doped and un-doped graphene sheets. As found in DFT calculations of O_2 adsorption on

carbon nano tubes (CNTs) [22,23] and N-doped graphite [16], there is a barrier for the adsorption. However the difference of the stable spin state between reactant (triplet) and product (singlet) makes the examination of the barrier complicated. According to ref. [23], spin non-polarized DFT calculations can properly treat the adsorption of an O_2 molecule on CNTs when the molecule is near the surface. The adsorption energy E_{ads} is defined as follows:

$$E_{\text{ads}} = E(O_2 \text{ on } C_{32-m}N_m) - E(C_{32-m}N_m) - \mu_{O_2}$$

Calculated energies are listed in Table 1. We found that the endothermicity of O_2 adsorption on the N-doped graphene sheet becomes dramatically lower as the number of N in the model increases and the adsorption finally becomes exothermic in the N3 and N4 models. This indicates the decrease in the repulsive interaction between an O_2 and N-doped graphene sheet. Note that O_2 adsorption on the N4 model is exothermic even when the Gibbs free energy correction for O_2 gas in the standard state (0.44 eV) is taken into account.

We consider that the decrease in the repulsive interaction between an O_2 and N-doped graphene sheet results from charge transfer in the sheet. The C–N bonds polarize into $C(\delta^+)-N(\delta^-)$ from the difference in electronegativity of C (2.5) and N (3.0) determined by Pauling. This suggests that the repulsive interaction between graphene π electrons and lone pair electrons of O_2 molecules becomes weaker as the number of N that bond with $C=C$ on which the O_2 molecule is adsorbed becomes larger.

According to Table 1, the bond length of $C=C$ on which O_2 is adsorbed is 1.54–1.58 Å, which shows that it is a single bond rather than a double bond. The bond length of O–O is 1.49–1.60 Å. This indicates that the O–O bond is longer than the isolated O_2 molecule (1.25 Å as obtained from a DFT calculation) and is comparable to the bond in $HOOH$ (1.48 Å), which suggests an inflow of electrons from the graphene sheet to O_2 . The bond lengths of C–O (1.46–1.67 Å) are somewhat longer than that of O in CH_3-O-CH_3 (1.42 Å). However, the length is much shorter than the sum of van der Waals radii of C and O (3.22 Å). These results evidently show that O_2 molecules are chemisorbed on the graphene sheets in the present model, although the chemisorption may be metastable relative to the N-doped (N-un-doped) graphene sheet plus O_2 asymptote.

3.3. ORR pathways on N-doped carbon

The ORR pathway on the N2-A model was examined in FPMD simulations. We chose the N2-A model because aromatic compounds such as pyrazine ($C_4N_2H_4$) and 2,2'-bipyridine ($C_{10}N_2H_8$) contain the *cis* conformation of N atoms with respect to a $C=C$ bond in the model (Fig. 1), which might be useful for synthesizing N-doped graphene sheets with controlling the arrangement of the N atoms.

A model of the catalyst/water interface consisting of the N2-A model with an O_2 molecule on it and a well equilibrated water slab obtained from a previous simulation [15] to include the solvent effects was annealed at 353 K for 1.7 ps. We found that two C–O bonds were maintained up to around 0.7 ps. After that, one O atom moved upward and the other remained bound with a C atom. Hereafter, the former and latter O atoms are designated as O_A and O_B , respectively. An H was then added to an H_2O in the water slab to introduce a proton (H_3O^+) into the computational cell. At around 34 fs, the O_A abstracted an H from a solvent H_2O molecule and $O_B O_A H_{\text{ads}}$ and OH_{aq}^- formed (Fig. 2a). Through the proton relay mechanism, $H_3O_{\text{aq}}^+$ and OH_{aq}^- approached each other in the water slab and they recombined at around 194 fs as shown in Fig. 2b. While the O_B-OAH bond vibrated for some time, the bond became longer after 600 fs as shown in Fig. 3, and it finally broke (Fig. 2c). Thus, the first FPMD simulation for ORR resulted in O_B on the N-doped graphene sheet and OAH_{aq}^- in the water slab. Note that the

Table 1

Formation energy of nitrogen doping E_F , O_2 adsorption energy E_{ads} (in eV), $C=C$ bond length on which O_2 is adsorbed $R(C=C)$, O_2 bond length $R(O-O)$, and C–O bond length $R(C-O)$ (in Å).

	E_F	E_{ads}	$R(C=C)$	$R(O-O)$	$R(C-O)$
N0	–	2.21 (2.65) ^{**}	1.54	1.51	1.50
N1	1.11 (1.29) [*]	1.08 (1.52) ^{**}	1.54	1.50	1.48, 1.55 ^{***}
N2-A	0.90 (1.26) [*]	0.06 (0.50) ^{**}	1.55	1.49	1.52
N2-B	0.85 (1.21) [*]	0.06 (0.50) ^{**}	1.55	1.49	1.52
N2-C	0.99 (1.35) [*]	0.26 (0.70) ^{**}	1.54	1.49	1.44, 1.67 ^{***}
N3	0.90 (1.44) [*]	-0.26 (0.18) ^{**}	1.56	1.49	1.48, 1.54 ^{***}
N4	0.88 (1.60) [*]	-0.57 (-0.13) ^{**}	1.58	1.60	1.46

* Values in parentheses mean the formation energy including the correction of the Gibbs free energy for N_2 gas in the standard state (0.36 eV/molecule).

** Values in parentheses mean the O_2 adsorption energy including the correction of the Gibbs free energy for O_2 gas in the standard state (0.44 eV/molecule).

*** There are two C–O bonds because the adsorption structure is asymmetric.

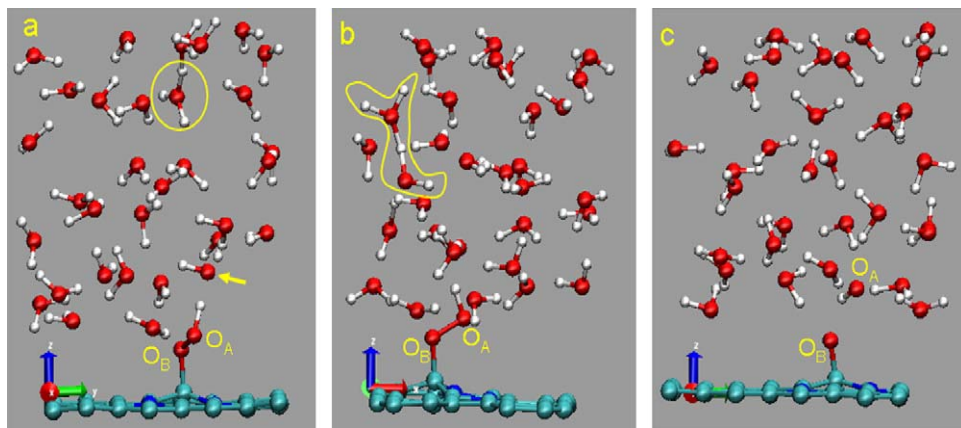


Fig. 2. Snapshots of the first FPMD simulation for ORR. Red, white, blue, and sky blue balls and sticks, respectively, represent O, H, N, and C atoms. (a) O_BO_AH and OH_{aq}⁻ (arrow) formed at 34 fs. (b) Neutralization of OH_{aq}⁻ with H₃O_{aq}⁺ at 194 fs. (c) O_B on the sheet and O_AH₂O⁻ finally formed at 1210 fs. (For interpretation of the references to color in this figure legend, the reader is referred to the web version of the article.).

formations of O_BO_AH_{ads} and O_AH_{aq}⁻ correspond to the first and second ORR step, respectively.

In this simulation, there was one proton in the initial state and it disappeared after the reaction. This may cause a sudden change of the electrode potential during the reaction. To control the change, the reaction was examined with a quadruple cell that contains one oxygen molecule, four protons, 124 water molecules, and an N-doped graphene sheet (C₁₂₆N₂) in the initial state. It was confirmed that the result of the quadruple cell was essentially consistent with that of the original cell, although OOH_{ads} appeared more transiently in the quadruple cell because of the immediate bond breaking of O-OH.

The first and second reduction steps on the N2-A model was quite different from the ones on Pt(1 1 1) [11] and Pt₂ dimer [15]. The ab-initio molecular dynamics simulation by Wang and Balbuena showed that OOH_{ads} on Pt(1 1 1) spontaneously and immediately decomposes into O_{ads} and OH_{ads} [11]. Moreover, OOH_{ads} on Pt₂ dimer embedded in a graphene sheet remains intact and the O-OH bond did not break in the FPMD simulation [15].

We considered that O-OH bond-breaking reaction (OOH_{ads} + e⁻ → O_{ads} + OH_{aq}⁻) is a key to 4e⁻ reduction because the breakage of the bond imposes significant restrictions on possible subsequent reaction paths. We confirmed the occurrence of the breakage by doing another three MD runs with different initial geometries. As described in Section 3.4, the breakage was also supported from a thermochemical analysis.

We found that the O_AH_{aq}⁻ ion can be neutralized into H₂O by adding a proton to the water slab. The further reduction step was examined by adding another proton to the water slab as shown in Fig. 4a. The O_B reacted with a proton through the proton relay

mechanism (Fig. 4b), and O_BH_{ads} formed (Fig. 4c). We continued the simulation up to 2.9 ps and found that O_BH_{ads} remains on the graphene sheet without desorbing from the sheet as O_BH_{aq}⁻ ion. After that, we confirmed that the fourth reduction step O_BH_{ads} → H₂O immediately occurs when another proton is added to the water slab. Thus, the FPMD simulations indicated that the ORR pathway for the 4e⁻ reduction on the N2-A model is as follows: O₂ads → OOH_{ads} → O_{ads} + OH_{aq}⁻ → O_{ads} + H₂O_{liq} → OH_{ads} + H₂O_{liq} → 2H₂O_{liq}.

In a direct MD simulation, one cannot sample all possible pathways and also cannot completely rule out the possibility that one have captured an extremely rare event, however in the present particular case, different simulations provided essentially the same pathway for the ORR on N-doped carbon: ORR at the zigzag edge of N-doped graphite examined by using a thermodynamic integration methodology [16]. We also obtained the same pathway in a similar MD simulation of ORR on N2-B model. The agreement of the predicted pathway suggests that it captures an essential feature of ORR on N-doped carbons.

It should be noted that OOH_{ads}, the product of the first reduction, retained its O-O bond for 600 fs (Fig. 3). When we advanced to the second reduction step before the O-OH bond broke, we found that HOOH formed. This is the same ORR pathway as calculated on Pt₂ dimer embedded in a graphene sheet [15]. These results indicate that not only the 4e⁻ reduction but also the 2e⁻ reduction will occur on the N-doped graphene sheet.

3.4. Possible branching in ORR path on N2-A model

To forward the reaction in a direct simulation within a few picoseconds, the electrode potential may be set in low compared to experimental situations. This might cause a deviation from the reaction path at high electrode potential. The validity of the path obtained from the FPMD simulation can be assessed based on a thermochemical analysis combined with static DFT calculations. As shown in Fig. 5, we considered alternative intermediates that were not found in the FPMD simulation and possible branching paths. It is worthy of note that the bond-breaking reaction of OOH_{ads} + e⁻ → O_{ads} + OH_{aq}⁻ plays an important role in ORR of N-doped carbon because the reaction significantly restricts the subsequent ORR path (Fig. 5). We show that the occurrence of the reaction is plausible in terms of thermochemistry as well as the FPMD simulation. The stability of three intermediates A-C (A: OOH_{aq}⁻, B: O_{ads} + OH_{aq}⁻, and C: O_{ads} + OH_{ads} + e⁻) were compared using thermochemical data [24], standard electrode potentials [25], and the adsorption energies obtained from the static DFT calculations. In the following, G(X_α) stands for Gibbs energy of X in

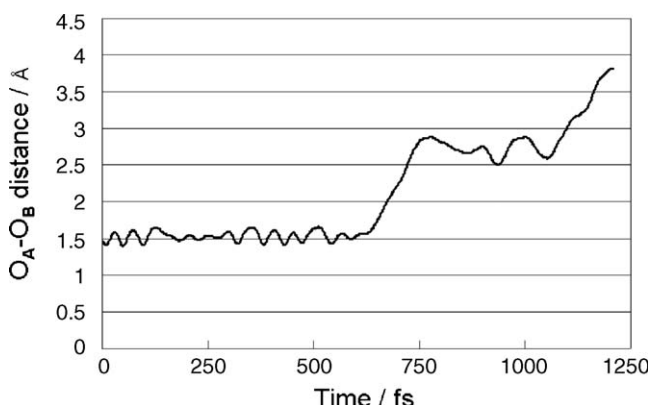


Fig. 3. Time evolution of O_A-O_B distance in the first FPMD simulation for ORR.

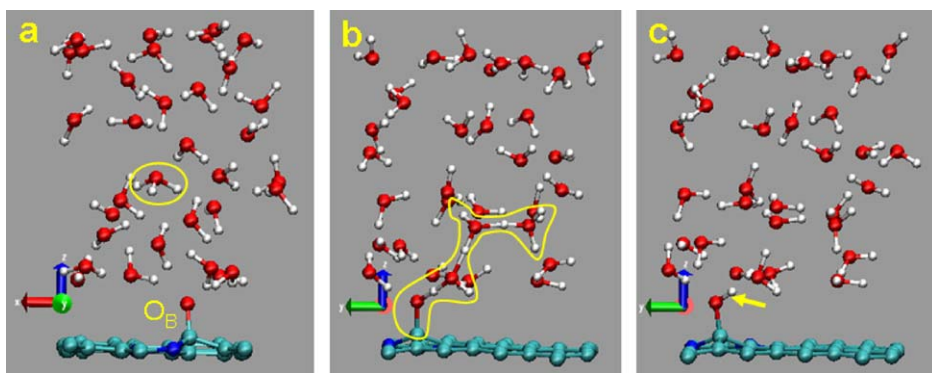
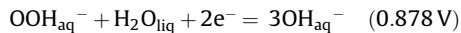
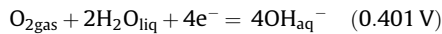


Fig. 4. Snapshots of FPMD simulation of third ORR step. Red, white, blue, and sky blue balls and sticks, respectively, represent O, H, N, and C atoms. (a) Initial state. (b) Proton attacks O_B through proton relay mechanism at 91 fs. (c) O_BH formed on sheet at 121 fs. (For interpretation of the references to color in this figure legend, the reader is referred to the web version of the article.).

a state α at the standard state. The adsorption energy of Y on the surface ($G_{\text{ads}}(Y)$) was defined as follows:

$$G_{\text{ads}}(Y) \equiv G(Y_{\text{gas}}) + G(\text{surface}) - G(Y_{\text{ads}}).$$

$G(OH_{\text{aq}}^-)$ and $G(OOH_{\text{aq}}^-)$ needed to compare the stability of three states A–C can be evaluated by combining thermochemical data of $G(O_{2\text{gas}})$ and $G(H_2O_{\text{liq}})$ [24] with the standard electrode potential of the following two reactions [25].



We get $-(2.149 + U_{\text{ABS}})$ eV and $-(1.512 + U_{\text{ABS}})$ eV for $G(OH_{\text{aq}}^-)$ and $G(OOH_{\text{aq}}^-)$, respectively. Here, U_{ABS} stands for the absolute electrode potential that is related to standard hydrogen electrode (SHE) and the vacuum level. Using thermochemical data of $G(O_{\text{gas}})$ [24], the energy of the state B is given as follows:

$$\begin{aligned} G(O_{\text{ads}}) + G(OH_{\text{aq}}^-) &= G(O_{\text{gas}}) - G_{\text{ads}}(O) + G(OH_{\text{aq}}^-) \\ &= -(0.064 + G_{\text{ads}}(O) + U_{\text{ABS}}) \text{ eV}. \end{aligned}$$

$G_{\text{ads}}(O)$ of 3.261 eV was obtained from a static DFT calculation with including the contribution from translational entropy of O atom in gas phase (0.442 eV) at the standard state. Note that the contribution from $G(\text{surface})$ to the energy can be offset in the comparison. Thus, we found that the state B is thermochemically more stable than the state A, i.e., $G(OOH_{\text{aq}}^-)$ by 1.81 eV.

Next, we examine the condition of the electrode potential (U_{SHE}) in a SHE scale where the state B is more stable than the state C. DFT calculation with including the contributions from translational entropy of O atom (0.442 eV) and OH radical (0.447 eV) in gas phase at the standard state provides $G_{\text{ads}}(O + OH)$ of 4.062 eV. The energy of the state C is given as follows:

$$\begin{aligned} G(O_{\text{gas}}) + G(OH_{\text{gas}}) - G_{\text{ads}}(O + OH) - e \times (U_{\text{SHE}} + U_{\text{ABS}}) \\ = -(2.141 + U_{\text{SHE}} + U_{\text{ABS}}) \text{ eV}. \end{aligned}$$

Therefore, the state B is more stable than the state C when U_{SHE} is lower than 1.18 V. This thermochemical analysis shows that the bond-breaking reaction is a plausible path in ORR on N-doped carbon.

In a similar manner, we found that $(O_{\text{ads}} + H_2O_{\text{liq}})$ is more stable than $(OH_{\text{ads}} + OH_{\text{ads}})$ and $HOOH_{\text{aq}}$ by 0.59 and 1.95 eV, respectively. We also found that $(OH_{\text{ads}} + e^-)$ is more stable than OH_{aq}^- when U_{SHE} is higher than 0.43 V. These results support the relevance of the MD path. It should be noted that $(O_{\text{ads}} + O_{\text{ads}})$ is slightly more stable than $O_{2\text{ads}}$ by 0.19 eV. However, unlike the case of the N4 model as stated below, the O–O bond did not spontaneously break on the N2-A model in the FPMD simulation.

3.5. Reversible potential of each reduction step

Having obtained a qualitative ORR pathway for $4e^-$ reduction on the N2-A model, we are now in a position to consider the semi-quantitative aspects of ORR. By comparing the energies of the reactant, intermediates, and product, we obtained the reversible potential of each elementary reduction. To compare the energies of each state, we first adjusted the stoichiometry of each state by adding protons in an aqueous environment, and electrons in a similar manner as was done in ref. [26]:

Reactant : $G(O_{2\text{gas}}) + 4G(H_{\text{aq}}^+) - 4e \times U$

Intermediate1 : $G(OOH_{\text{ads}}) + 3G(H_{\text{aq}}^+) - 3e \times U$

Intermediate2 : $G(O_{\text{ads}}) + G(OH_{\text{aq}}^-) + 3G(H_{\text{aq}}^+) - 2e \times U$

Intermediate3 : $G(O_{\text{ads}}) + G(H_2O_{\text{liq}}) + 2G(H_{\text{aq}}^+) - 2e \times U$

Intermediate4 : $G(OH_{\text{ads}}) + G(H_2O_{\text{liq}}) + G(H_{\text{aq}}^+) - e \times U$

Product : $2G(H_2O_{\text{liq}})$

Here, U stands for the electric potential and it decomposes into U_{SHE} and U_{ABS} , i.e. $U = U_{\text{SHE}} + U_{\text{ABS}}$. Thus, the energy of the reactant and intermediates depends on U_{SHE} .

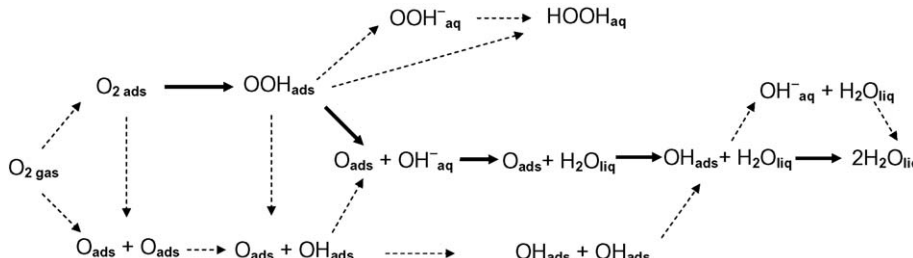


Fig. 5. Possible intermediates and paths in ORR. Arrows in solid line corresponds to $4e^-$ reduction pathway found by FPMD simulations.

As was done in the previous subsection, $G(Y_{\text{ads}})$ in the intermediates can be rewritten by the adsorption energy $G_{\text{ads}}(Y)$. $G(\text{H}_{\text{aq}}^+)$ and U_{ABS} can be eliminated from the reactant and intermediates by using the equilibrium condition of H_{aq}^+ with H_2 gas in the standard state:

$$G(\text{H}_{\text{aq}}^+) - e \times U_{\text{ABS}} = 1/2G(\text{H}_{2\text{gas}}).$$

Since the product ($2\text{H}_2\text{O}_{\text{liq}}$) contains no additional protons and electrons to adjust the stoichiometry, we calculated the relative energy of each state from the product. This treatment is convenient for offsetting a contribution from the Gibbs energy of surface $G(\text{surface})$. Thus, the relative energy of the reactant and intermediates can be represented as follows:

$$\text{Reactant} : G(\text{O}_{2\text{gas}}) + 2G(\text{H}_{2\text{gas}}) - 4e \times U_{\text{SHE}} - 2G(\text{H}_2\text{O}_{\text{liq}})$$

$$\begin{aligned} \text{Intermediate1} : & G(\text{OOH}_{2\text{gas}}) - G_{\text{ads}}(\text{OOH}) + 1.5G(\text{H}_{2\text{gas}}) \\ & - 3e \times U_{\text{SHE}} - 2G(\text{H}_2\text{O}_{\text{liq}}) \end{aligned}$$

$$\begin{aligned} \text{Intermediate2} : & G(\text{O}_{\text{gas}}) - G_{\text{ads}}(\text{O}) + G(\text{H}_{2\text{gas}}) + G(\text{OH}_{\text{aq}}^-) \\ & + G(\text{H}_{\text{aq}}^+) - 2e \times U_{\text{SHE}} - 2G(\text{H}_2\text{O}_{\text{liq}}) \end{aligned}$$

$$\begin{aligned} \text{Intermediate3} : & G(\text{O}_{\text{gas}}) - G_{\text{ads}}(\text{O}) + G(\text{H}_{2\text{gas}}) - 2e \times U_{\text{SHE}} \\ & - G(\text{H}_2\text{O}_{\text{liq}}) \end{aligned}$$

$$\begin{aligned} \text{Intermediate4} : & G(\text{OH}_{\text{gas}}) - G_{\text{ads}}(\text{OH}) + 0.5G(\text{H}_{2\text{gas}}) \\ & - e \times U_{\text{SHE}} - G(\text{H}_2\text{O}_{\text{liq}}) \end{aligned}$$

We made the following assumptions for the sake of simplicity. In evaluating Gibbs energy change $G_{\text{ads}}(X)$, we used the Kohn-Sham (KS) energy change under a perfect vacuum condition with including a correction from translational entropy of X in gas at the standard state. We used thermochemical data for $G(\text{O}_{2\text{gas}})$, $G(\text{H}_{2\text{gas}})$, $G(\text{H}_2\text{O}_{\text{liq}})$, $G(\text{O}_{\text{gas}})$, and $G(\text{OH}_{\text{gas}})$ [24]. $G(\text{OH}_{\text{aq}}^-)$ was evaluated in the same manner as Section 3.4. Because $G(\text{OOH}_{\text{gas}})$ was not available in ref. [24], we used $G(\text{OOH}_{\text{aq}})$ estimated from the standard electrode potential of $\text{O}_{2\text{gas}} + \text{H}_{\text{aq}}^+ + e^- \rightarrow \text{OOH}_{\text{aq}}$ (−0.13 V [25]) and we omitted a correction from translational entropy of OOH in gas phase in the computation of $G_{\text{ads}}(\text{OOH})$ to avoid the overcorrection.

The calculated relative energies are shown in Fig. 6. The potential at the intersection between two successive states corresponds to the reversible potential at each reduction step. The reversible potentials of the first, second, third, and fourth reductions are 0.58, 1.90, 0.34, and 1.26 V, respectively (Table 2). High reversible potential is a desirable character for ORR catalysts. The reversible potential of the fourth reduction ($\text{OH}_{\text{ads}} + \text{H}_{\text{aq}}^+ + e^- \rightarrow \text{H}_2\text{O}_{\text{liq}}$) is significantly high. This indicates that OH poisoning is unlikely on the N4 model. By contrast, the third reduction ($\text{O}_{\text{ads}} + \text{H}_{\text{aq}}^+ + e^- \rightarrow \text{OH}_{\text{ads}}$) might be a rate-determining step of the ORR on the model, because its reversible potential is the lowest. This shows that O_{ads} is stable unless the electric potential is significantly low ($U_{\text{SHE}} < 0.34$ V). Thus, O_{ads} may act as a poison for the ORR on the N2-A model. Note that all reduction steps become exothermic when we set the potential below the minimum reversible potential (0.34 V). However, the electromotive force of the fuel cell will be small in such a condition.

As listed in Table 2, we also calculated the reversible potential of each ORR step on the zigzag edge of N-doped graphite that corresponds to the e-1 model in ref. [16]. Judging from a slightly higher value in the minimum reversible potential on the edge model (0.39 V) than that on the N2-A model (0.34 V), the edge model is expected to show a marginally better catalytic activity than the N2-A model.

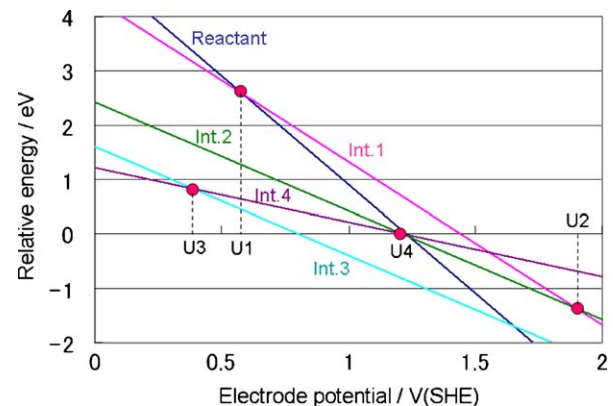


Fig. 6. Energy of reactant and four intermediates relative to product ($2\text{H}_2\text{O}_{\text{liq}}$) versus electrode potential measured from SHE (U_{SHE}). U_1 , U_2 , U_3 , and U_4 stand for the reversible potentials of the first, second, third, and fourth reductions, respectively.

3.6. ORR on N4 model

Finally, we examined ORR on the N4 model. We found that molecular adsorption of O_2 on the N4 model is metastable. The FPMD simulation showed that the O–O bond immediately and spontaneously broke on this model. We confirmed that the bond broke irrespective of the presence of solvent H_2O molecules in the simulation. The bond breaking reaction is exothermic by 2.52 eV (as obtained from a DFT calculation without solvent molecules), which suggests strong binding between O atoms and the N4 model.

We added an H to an H_2O in the water slab in order to add a proton to the computational cell. At around 120 fs one O_{ads} was reduced to OH_{ads} , as shown in Fig. 7a. After the first ORR, the second reduction was examined. The other O_{ads} was also reduced to OH_{ads} (Fig. 7b and c) through the proton relay mechanism. Although we tried the third reduction, no reaction occurred in the FPMD simulations with one proton in the computational cell. We also tried a simulation that started with two protons in the water slab, as was done to examine the ORR on Pt_2 dimer [15]. However, the simulation results in isomerization of the adsorbate ($\text{OH}_{\text{ads}} + \text{O}_{\text{H-ads}} \rightarrow \text{O}_{\text{ads}} + \text{H}_2\text{O}_{\text{liq}}$) rather than a reduction. An evaluation of thermochemical stability of $(\text{OH}_{\text{ads}} + \text{OH}_{\text{ads}})$ and $(\text{O}_{\text{ads}} + \text{H}_2\text{O}_{\text{liq}})$, as was done in Section 3.4, showed that the latter is more stable than the former by 0.70 eV.

The difficulty in advancing the third reduction ($\text{O}_{\text{ads}} + \text{H}_{\text{aq}}^+ + e^- \rightarrow \text{OH}_{\text{ads}}$) can be explained from the reversible potential of each reduction step. The calculated potentials of the second and third reductions are 0.24, and −0.47 V, respectively. The low reversible potential of the third reduction suggests O poisoning on the N4 model. From the calculation of the reversible potential, we found that the N3 model also suffers from a similar O poisoning (−0.50 V).

Although the N4 and N3 models seem to be superior to the N2 models with respect to adsorbing O_2 molecules, as shown in Table 1, much too affinity for oxygen results in O poisoning in the N4 and N3 models. This tends to prohibit $4e^-$ reduction on these models.

Table 2

Reversible potential of four elementary ORR steps on basal plane model (N2-A) and on edge model that corresponds to $e-1$ in ref. [16] (in V/SHE).

Step	Reaction	Basal plane (N2-A)	Edge (e-1)
1	$\text{O}_{2\text{ads}} + \text{H}_{\text{aq}}^+ + e^- \rightarrow \text{OOH}_{\text{ads}}$	0.58	0.72
2	$\text{OOH}_{\text{ads}} + e^- \rightarrow \text{O}_{\text{ads}} + \text{OH}_{\text{aq}}^-$	1.90	1.97
3	$\text{O}_{\text{ads}} + \text{H}_{\text{aq}}^+ + e^- \rightarrow \text{OH}_{\text{ads}}$	0.34	0.39
4	$\text{OH}_{\text{ads}} + \text{H}_{\text{aq}}^+ + e^- \rightarrow \text{H}_2\text{O}_{\text{liq}}$	1.26	1.01

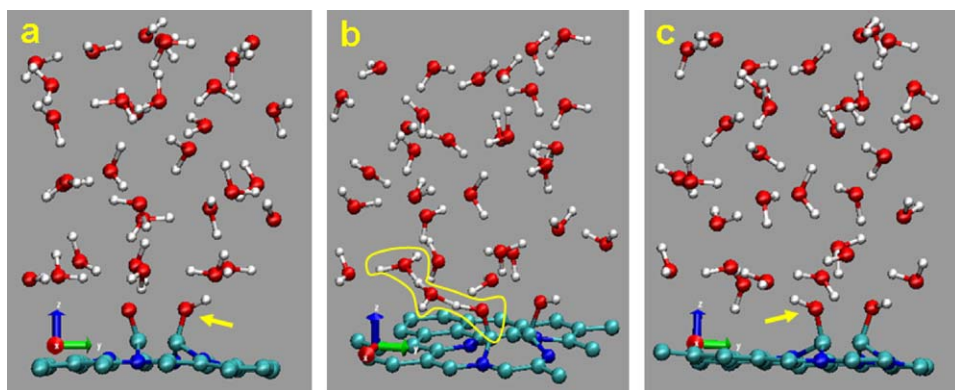


Fig. 7. Snapshots of FPMD simulation of ORR on N4 model. Red, white, blue, and sky blue balls and sticks, respectively, represent O, H, N, and C atoms. (a) Product of first ORR step at 120 fs. (b) Second ORR step. A proton attacks O_{ads} through the proton relay mechanism at 104 fs. (c) Another OH_{ads} formed on the N4 model at 139 fs. (For interpretation of the references to color in this figure legend, the reader is referred to the web version of the article.).

4. Summary

Density-functional calculations were performed to investigate oxygen reduction reactions (ORRs) on N-doped carbon. Graphene sheets having one to four N impurities in the substitutional site of C around a C=C bond were examined as model structures. We found that the binding interaction between graphene and O₂ becomes stronger as the number of N atoms bonding with the C=C increases. We performed a series of FPMD simulations to elucidate the ORR pathway on N-doped graphene. We found a path to 4e⁻ reduction that leads to H₂O formation. However, if the second reduction occurs before the O-OH bond breaks, there is a path to 2e⁻ reduction that results in the unfavorable product, HOOH. Calculations of the reversible potential of each reduction step in relation to the determined pathways showed that reduction of O intermediate requires a low electrode potential, which indicates the possibility of poisoning by the intermediate on N-doped graphene sheets.

Acknowledgements

The author thanks O. Sugino, M. Otani, Y. Morikawa, I. Hamada, N. Watari, and T. Ikeshoji for their useful discussions. Calculations were made using the Earth Simulator at the Earth Simulator Center, Yokohama, Japan and the Hitachi SR11000 in the supercomputing center at the University of Tokyo. Part of this research was performed by “Advanced Large-scale Computational Simulation Services” supported by Open Advanced Facilities Initiative for Innovation (Strategic Use by Industry) of the Ministry of Education, Culture, Sports, Science and Technology (MEXT) of Japan.

References

- [1] J.O'M. Bockris, U.M. Shahed, *Surface Electrochemistry*, Plenum Press, New York, 1993.
- [2] A. Wieckowski (Ed.), *Interfacial Electrochemistry*, Marcel Dekker, Inc., New York, 1999.
- [3] J. Lipkowski, P.N. Ross, *Electrocatalysis*, Wiley-VCH, New York, 1998.
- [4] J. Zagal, P. Bindra, E. Yeager, *J. Electrochem. Soc.* 127 (1980) 1506.
- [5] R. Bashyam, P. Zelenay, *Nature* 443 (2006) 63.
- [6] R.A. Sidik, A.B. Anderson, N.P. Surbramanian, S.P. Kumaraguru, B.N. Popov, *J. Phys. Chem. B* 110 (2006) 1787.
- [7] J. Ozaki, T. Anahara, N. Kimura, A. Oya, *Carbon* 44 (2006) 3358.
- [8] J. Rossmeisl, A. Logadottir, J.K. Nørskov, *Chem. Phys.* 319 (2005) 178.
- [9] Y. Ishikawa, J.J. Mateo, D.A. Tryk, C.R. Cabrera, *J. Electroanal. Chem.* 607 (2007) 37.
- [10] D. Cao, G.-Q. Lu, A. Wieckowski, S.A. Wasileski, M. Neurock, *J. Phys. Chem. B* 109 (2005) 11622.
- [11] Y. Wang, P.B. Balbuena, *J. Phys. Chem. B* 108 (2004) 4376.
- [12] M. Otani, O. Sugino, *Phys. Rev. B* 73 (2006) 115407.
- [13] O. Sugino, I. Hamada, M. Otani, Y. Morikawa, T. Ikeshoji, Y. Okamoto, *Suf. Sci.* 601 (2007) 5237.
- [14] M. Otani, I. Hamada, O. Sugino, Y. Morikawa, Y. Okamoto, T. Ikeshoji, *J. Phys. Soc. Jpn.* 77 (2008) 024802.
- [15] Y. Okamoto, *J. Phys. Chem. C* 112 (2008) 5888.
- [16] T. Ikeda, M. Boero, H. Sheng-Feng, K. Terakura, M. Oshima, J. Ozaki, *J. Phys. Chem. C* 112 (2008) 14706.
- [17] Y. Morikawa, K. Iwata, K. Terakura, *Appl. Surf. Sci.* 169 (2001) 11.
- [18] J.P. Perdew, K. Burke, M. Ernzerhof, *Phys. Rev. Lett.* 77 (1996) 3865.
- [19] D. Vanderbilt, *Phys. Rev. B* 41 (1990) 7892.
- [20] S.G. Louie, S. Froyen, M.L. Cohen, *Phys. Rev. B* 26 (1982) 1738.
- [21] D.R. Lide (Ed.), *CRC Handbook of Chemistry and Physics*, 82nd ed., CRC Press, Boca Raton, 2001, pp. 5–35.
- [22] D.C. Sorescu, K.D. Jordan, P. Avouris, *J. Phys. Chem.* 105 (2001) 11227.
- [23] S.-P. Chan, G. Chen, X.G. Gong, Z.-F. Liu, *Phys. Rev. Lett.* 90 (2003) 086403.
- [24] I. Barin (Ed.), *Thermochemical Data of Pure Substances*, VCH, Weinheim, 1989.
- [25] The Chemical Society of Japan, *Handbook of Chemistry*, 3rd ed., Maruzen, Tokyo, 1984, p. II-475 (Kagaku-binran in Japanese).
- [26] Y. Okamoto, *Appl. Surf. Sci.* 255 (2008) 3434.